N O T I C E

THIS DOCUMENT HAS BEEN REPRODUCED FROM MICROFICHE. ALTHOUGH IT IS RECOGNIZED THAT CERTAIN PORTIONS ARE ILLEGIBLE, IT IS BEING RELEASED IN THE INTEREST OF MAKING AVAILABLE AS MUCH INFORMATION AS POSSIBLE

A Spectroscopic Study of Intermediates in the Condensation of Refractory Smokes: Matrix Isolation Experiments on SiO

by

R. K. Khanna and D. D. Stranz
Department of Chemistry, University of Maryland
College Park, Maryland 20742
and
B. Donn
Laboratory of Extraterrestrial Physics
Goddard Space Flight Center, Greenbelt, Maryland 20771

Abstract

The infrared and Raman spectra of N_2 matrix-isolated silicon oxides were investigated. The vibrational frequencies of SiO, Si_2O_2, and Si_3O_3 were identified and assigned on the basis of normal coordinate analyses. Heating the solid to ~50K (evaporating the matrix) leaves a residue whose infrared spectrum is identical to that of a smoke condensed at ambient temperatures. Further heating of the sample to ~500K leads to significant changes in the band shapes. Investigations of the infrared spectra at several stages of the diffusion process enabled us to propose a mechanism for the transition from molecular properties to those of the residue (bulk) material, which has been characterized as Si_2O_3.

Introduction

Condensation of multielement refractory grains from interstellar molecules seems to be a common phenomenon in our galaxy. Although the reverse process, vaporization, has been extensively investigated [1-3] in the laboratory, the formation of small grains, or smoke, from condensing vapors has not been studied in as much detail. For example, in the

reported studies of the condensation of Al_2O_3 and other oxides [3], the principal interest was in characterization of the final products rather than the mechanism and intermediates of condensation.

Recently, Donn and his associates initiated experimental and theoretical research on grain formation relevant to cosmic systems. Their first experiments involved SiO smoke formation by vaporizing the material in a few torr of inert buffer gas [4]. The infrared spectra of the amorphous grains condensed are practically identical to those of a material characterized in the literature as Si_2O_3 [5,6]. The co-condensation of Mg and SiO vapors under similar conditions in their experiments produced grains with variable Mg/Si ratios which upon high temperature annealing were converted to Mg_2SiO_4 (forsterite) [7].

The conditions in astrophysical systems where grain formation occurs differ considerably from those which must be employed in the laboratory to obtain useful results in a reasonable time. In order to apply experimental results to astrophysics, a knowledge of the condensation mechanism is required. Under the laboratory conditions used in the smoke formation experiments described above, the condensation is extremely fast (a few microseconds); consequently, it is difficult to detect and determine the nature of any intermediate molecular species. However, low temperature matrix isolation techniques permit the quenching of the vapor in an inert gas solid and controlling the polymerization of the trapped molecules by raising the temperature of the matrix to the point at which slow diffusion and reaction may occur. By varying the duration and conditions of the diffusion period, the unstable intermediates of the condensation process can be immobilized for spectroscopic study. The matrix isolation technique has been extensively employed [8-10] in the study of molecular or radical species which are unstable under ambient conditions, and is finding highly productive and successful use in the examination of trapped vapors of high temperature solids and the controlled growth of multimeric structures from diffusing monomers [11,12]. We present here the results of our infrared and Raman spectroscopic studies of the condensation of SiO molecules in low

temperature nitrogen matrices and the effects of controlled warm-up from 12 to 500K.

The literature shows one brief and two fairly detailed reports on the infrared spectra of matrix isolated silicon oxide species [13-15]. Anderson, et. al. [13], and Anderson and Ogden [14], employing N_2 and Ar matrices, identified features due to monomeric (SiO), dimeric (Si_2O_2), and trimeric (Si_3O_3) species. Using isotopic data from ^{18}O-enriched samples, they interpreted their spectra on the basis of closed cyclic structures (point groups D_{2h} and D_{3h} for dimer and trimer respectively) containing only Si-O bonds. Normal coordinate analyses for these structures were carried out by these authors to check the frequency assignments and to predict the frequencies of the infrared inactive modes. Hastie, et. al. [15] investigated the spectra in Ar and Ne solids, and assigned additional peaks to pentameric SiO species as well as confirming those features assigned by Anderson and Ogden. A double hexagonal ring structure (similar to napthalene) for the pentamer was proposed by these authors on the basis of the infrared data. Recently, Anderson [16] has carried out theoretical calculations on the binding energies of $(SiO)_n$ units, and has concluded that the most energetically favored species have Si-Si bonds. This implies at least a pseudo-linear structure for the SiO dimer, while the trimer would be quite asymmetric.

The structural conclusions proposed by Anderson and Ogden and by Hastie et. al. are based on incomplete vibrational spectra (only two of six frequencies for the dimer and three of seven expected distinct fundamentals for a D_{3h} trimeric species). At the same time, the theoretical structures proposed by Anderson are inconsistent with the observed infrared data as will be discussed in a later section. It was therefore felt desirable to reinvestigate the infrared spectra of matrix isolated $(SiO)_n$ species under high resolution and attempt to obtain Raman spectra as well (in spite of the anticipated weakness of scattering for the silicate structures). A third aim of our study was to extend the use of controlled diffusion and reaction in a low temperature matrix to parallel the formation of amorphous

grains as obtained by Donn and Day [4,7] in the gas phase, and to understand the mechanism for the formation of such grains.

Experimental Techniques

The low temperatures used in these experiments were obtained using a CTi model 21 closed-cycle helium cryocooler, which produces a base operating temperature near 12K. For infrared work, a CsI window mounted to the cold finger was used as a matrix substrate, while for the Raman experiments, the matrix was deposited on a highly polished brass plate substituted for the CsI window. A small heater wire wound around the substrate holder base was used to vary the temperature between 12 and 60K for diffusion studies. Substrate temperature was monitored with a 0.07 atomic % iron-doped gold versus chromel thermocouple sandwiched between the substrate plate and holder. A mixture of 1:1 mole ratio powdered elemental silicon and silicon dioxide (both obtained from Ventron) was vaporized at approximately 1300-1500K in a resistively heated alumina ceramic oven, and the vapors co-condensed with a stream of nitrogen gas onto the substrate, which was maintained at 15-20K during deposition. The leak rate of the nitrogen was controlled through a needle valve to vary the N_2:(SiO) ratio. Depositions were generally carried out over a 4-8 hour period to obtain optimum spectral intensities. Infrared spectra were recorded from 2000 cm^{-1} to 200 cm^{-1} on a Perkin-Elmer 225 grating spectrophotometer under typical resolution of 0.75 cm^{-1}. Raman spectra were recorded using a SPEX 1401 dual monochromator equipped with photon counting detection. Spectra were excited with the 488.0 and 514.5 nm lines from a Coherent Radiation model 52 argon ion laser. Typically, a resolution of 4 cm^{-1} was employed in the Raman studies.

Results

A series of experiments was performed to determine optimum conditions for deposition and isolation of monomeric, dimeric, and trimeric SiO species without background features due to higher polymeric molecules. The general features of the infrared spectra are similar to those reported by Anderson and Ogden [14], and as these researchers experienced, it does not seem possible to isolate solely monomeric SiO; surface diffusion during deposition always results in the formation of at least dimer and trimer. Depending on deposition conditions, and presumably on somewhat higher resolution and thicker matrix films from longer deposition times, some subtle differences from the published spectra of Anderson and Ogden and Hastie et. al. were noted. Tracings of the infrared and Raman spectra are reproduced in Figures 1-4. Raman data were particularly difficult to obtain since matrices intended for such examination were deposited on the brass plate, and, lacking facilities for reflection spectroscopy, infrared verification of the sample quality and concentration was prevented. It was also necessary to considerably reduce the laser power and defocus the beam to avoid burning holes in the sample or inducing diffusion in the laser spot.

Discussion

A. SiO

The assignment of the infrared features at 1224.4 cm^{-1}, 1216.5 cm^{-1}, and 1209.2 cm^{-1} is made to the monomers $^{28}Si^{16}O$, $^{29}Si^{16}O$, and $^{30}Si^{16}O$ respectively. This is consistent with the earlier matrix results of Hastie et. al. and Anderson and Odgen, and with gas phase data [17]. The Raman spectrum shows the peak due to $^{28}Si^{16}O$, the major isotopic species.

B. Si_2O_2

In the infrared spectrum, previously unreported, weak but reproducible features are observed at 1221.5 cm^{-1} and 1217.8 cm^{-1} which persist upon mild annealing. At lower frequencies, the peaks at 804.4 cm^{-1} and 765.5 cm^{-1} are strong. This pair has been assigned to the $^{28}Si_2^{16}O_2$ dimer by earlier researchers. Under all conditions where these two features appear with significant intensity, they are accompanied by less intense satellite peaks to lower frequencies, which vary in strength with the intensity of the stronger peaks. These satellites are attributed to various $(^{28}Si, ^{29}Si, ^{30}Si)_2O_2$ species, as is shown in Table 1. In the far infrared, a weak feature was observed at 252 cm^{-1} when the other dimer features were very intense. The 1221 cm^{-1}, 804 cm^{-1}, 765 cm^{-1}, and 252 cm^{-1} features exhibit similar changes in intensity with deposition conditions and upon diffusion in the matrix, and so are assigned to the $^{28}Si_2^{16}O_2$ dimer. In the Raman spectrum, a weak feature appears near 250 cm^{-1} which becomes weaker upon diffusion. The absence of other features which may be assigned to the dimer in the Raman spectrum may be explained by the low concentrations and an unfavorable scattering cross section. Hastie et. al. observed a strong absorption peak at 79 cm^{-1} which they associated with a torsional vibration of the dimer. Thus, five of the six fundamental modes of Si_2O_2 are observed in the infrared spectrum, with one coincidence in the Raman spectrum. The centrosymmetric D_{2h} structure proposed earlier is not consistent with these observations, since that symmetry permits only three infrared active modes and allows no coincidences between IR and Raman. On the basis of a simple valence force field, Anderson and Odgen predicted the Raman active modes of the D_{2h} model to be 774 cm^{-1} and 766 cm^{-1}. The failure to observe scattering near these frequencies, taken together with the 250 cm^{-1} coincidence between infrared and Raman spectra and the assignment of five IR features to a dimeric species is not supportive of the D_{2h} structure. Based on the theoretical atom superposition and electron delocalization MO calculations of Anderson [16], a centrosymmetric linear or bent Si-Si linked dimer is expected, which should exhibit a strong Raman active Si-Si symmetric stretch and an Si=O asymmetric stretch

in the infrared. In our experiments, no features are seen to support this type of bonding. In the chemistry of siloxane compounds, it is known that the Si-O bond is second in stability only to the Si-F bond [18]; in this respect, and considering the high temperature of the SiO units immediately prior to deposition in the matrix, it seems unlikely that a thermo-dynamically unstable isomer would form in appreciable concentration.

A rather unsymmetrical structure for the dimer is suggested by the appearance of five fundamentals. The peak at 1221 cm^{-1} implies an Si=O multiple bond, while the pair of peaks at 804 cm^{-1} and 765 cm^{-1} indicates two Si-O single bonds. Since on diffusion at 30K in the matrix, the Si_2O_2 concentration decreases rapidly, accompanied by an equally rapid increase of features due attributed to higher multimers, an open structure such as (I) or (II) below is likely:

(I)   (II)

In these structures, all four atoms are not necessarily coplanar. The high reactivity of the dimer is explained by the unsaturated end atoms, which should readily react with other SiO monomeric or dimeric species to form higher multimers. The D_{2h} structure would not be expected to have as high a reactivity, since each atom there has a filled octet and reaction involves breaking at least one Si-O bond. Reaction of the species (I) and (II) involves no bond breaking and little molecular rearrangement to form the trimer (which, as is discussed below, is a relatively stable D_{3h} structure), important considerations since little activation energy is available for reaction at 30K in a solid. Each of the structures (I) and (II) has three stretching, two bending, and one torsional vibrations, all of which are both IR and Raman active. The assignment of dimer features made above is consistent with both structures, including assignment of the

79 cm^{-1} feature to the torsion about the central Si=O bond. To check these structures and determine the most satisfactory, force constant refinement calculations were performed for both, using angles of 109.5° (tetrahedral) and 120°, and assuming a planar configuration. Of the four sets of force constants thus obtained, the most reasonable major and interaction force constants were obtained for structure (I) with tetrahedral bonds. It is to be understood that vibrational data alone are insufficient to give accurate information on bond angles, lengths, or planarity (or otherwise) of the configuration. Our molecular parameters and results for the $^{28}Si_2^{16}O_2$ species are given in Table 2 and the observed and calculated frequencies using these results for the major Si_2O_2 isotopic variants are shown in Table 1. The agreement between observed and calculated frequencies is reasonable considering the assumptions and uncertainties in structural parameters. The stretching force constants are also reasonable in comparison with those of stable siloxanes and silicates [18,19].

C. Si_3O_3

The previous researchers observed infrared features at 972 cm^{-1}, 631 cm^{-1}, and 311 cm^{-1}, which, based upon initial intensities and behaviour upon diffusion, were assigned to a cyclic D_{3h} trimer. We observed that these features, particularly the most intense 972 cm^{-1} peak, were extremely persistent during controlled diffusion studies. These features increased in intensity at the expense of primarily the dimer (the monomer decreased much more slowly) during mild diffusion; the 972 cm^{-1} peak was often 100% absorbing after a few hours of diffusion at 30K. When the matrix temperature was raised to the point at which slow sublimation of the nitrogen began, this feature remained visible as the last discrete peak before the bulk spectra predominated. This indicates a very stable structure. When the 972 cm^{-1} peak was totally absorbing, an additional weak feature at 621 cm^{-1} in the infrared was observed. Our Raman spectra showed a strong, resonance-enhanced peak at 675 cm^{-1} (with two overtones), another relatively strong peak at 458 cm^{-1}, and a weaker feature near 343 cm^{-1}. While measurements of intensity in matrix Raman experiments is

difficult primarily due to changes in the matrix structure and thus the
scattering with continued diffusion, these features nonetheless were
persistent and seemed to increase in intensity relative to other peaks
during diffusion at 30K. Due to intense background scattering, the lower
limit for our Raman spectra was about 150 cm^{-1}; however, Hastie et. al.
made infrared examination to 33 cm^{-1} and observed no absorptions
attributable to the trimer below the 311 cm^{-1} feature identified earlier.

These results indicate a strongly bonded, relatively stable and
symmetric trimer. The D_{3h} symmetry proposed by the first researchers
permits three IR active in-plane modes of E' symmetry, and an out-of-plane
mode of A_2" species. Two in-plane A_1' modes and the E' modes are Raman
active, along with a torsional mode of E" symmetry. An A_2' stretching mode
is inactive. The observed features are consistent with this symmetry, and
may be assigned as follows. The three strongest infrared features at 972
cm^{-1}, 631 cm^{-1}, and 311 cm^{-1} are assigned to the E' modes, while the 621
cm^{-1} peak is of species A_2". In the Raman, the 675 cm^{-1} progression and
the 458 cm^{-1} peak are assigned to the totally symmetric stretch and bend
respectively, and the 343 cm^{-1} feature is the E" torsion.

Anderson and Odgen [14] carried out a normal coordinate analysis for
the planar vibrations of the D_{3h} model using a simple force field
consisting of two major force constants and no interaction terms. They
were able to reproduce their observed spectra for the E' modes of the ^{16}O
and ^{18}O totally substituted species. For our analysis, an eight constant
force field was chosen to describe the stretching, bending, and torsional
forces and interactions. These are shown in Table 3. It should be noted
that the bend-bend interaction used assumes that "ortho" and "meta"
interactions are equal, while the "para" interactions are negligible.
This, along with some approximations concerning the structural parameters
affects the computed fit somewhat. Initial choices of numerical values for
these constants were based on the results of the dimer calculations and
anticipated results for the trimer. Anderson and Odgen assumed an O-Si-O
angle of 100° (Si-O-Si angle of 140°) in their analysis; to simplify

calculations, we adopted 120° for all bonds. A somewhat different choice of symmetry coordinates was also used to give better insight into the potential interaction terms. These are detailed below:

$$S_1 \ (A_1') = \ (1/\sqrt{6}) \ (\ \Delta r_1 + \Delta r_2 + \Delta r_3 + \Delta r_4 + \Delta r_5 + \Delta r_6 \ )$$

$$S_2 \ (A_1') = \ (1/\sqrt{6}) \ (\ \Delta\alpha_1 - \Delta\alpha_2 + \Delta\alpha_3 - \Delta\alpha_4 + \Delta\alpha_5 - \Delta\alpha_6 \ )$$

$$S_3 \ (A_2') = \ (1/\sqrt{6}) \ (\ \Delta r_1 - \Delta r_2 + \Delta r_3 - \Delta r_4 + \Delta r_5 - \Delta r_6 \ )$$

$$S_{4a} \ (E') = \ (1/\sqrt{6}) \ (2\Delta\alpha_1 - \Delta\alpha_3 - \Delta\alpha_5 \ )$$

$$S_{4b} \ (E') = \ (1/\sqrt{2}) \ (\ \Delta\alpha_3 - \Delta\alpha_5 \ )$$

$$S_{5a} \ (E') = \ (1/\sqrt{6}) \ (2\Delta\alpha_2 - \Delta\alpha_4 - \Delta\alpha_6 \ )$$

$$S_{5b} \ (E') = \ (1/\sqrt{2}) \ (\ \Delta\alpha_4 - \Delta\alpha_6 \ )$$

$$S_{6a} \ (E') = \ (1/\sqrt{12}) \ (2\Delta r_1 - \Delta r_2 - \Delta r_3 - \Delta r_4 - \Delta r_5 + 2\Delta r_6 \ )$$

$$S_{6b} \ (E') = \ (1/2) \ (\ \Delta r_2 + \Delta r_3 - \Delta r_4 - \Delta r_5 \ )$$

$$S_{7a} \ (E') = \ (1/\sqrt{12}) \ (-\Delta r_1 - \Delta r_2 + 2\Delta r_3 + 2\Delta r_4 - \Delta r_5 - \Delta r_6 \ )$$

$$S_{7b} \ (E') = \ (1/2) \ (-\Delta r_1 - \Delta r_2 + \Delta r_5 + \Delta r_6 \ )$$

$$S_8 \ (A_2'') = \ (1/\sqrt{6}) \ (\ \Delta\delta_1 - \Delta\delta_2 + \Delta\delta_3 - \Delta\delta_4 + \Delta\delta_5 - \Delta\delta_6 \ )$$

$$S_{9a} \ (E'') = \ (1/\sqrt{12}) \ (-\Delta\delta_1 + 2\Delta\delta_2 - \Delta\delta_3 - \Delta\delta_4 + 2\Delta\delta_5 - \Delta\delta_6 \ )$$

$$S_{9b} \ (E'') = \ (1/2) \ (\ \Delta\delta_1 - \Delta\delta_3 + \Delta\delta_4 - \Delta\delta_6 \ )$$

There is a built-in redundancy in the E' modes; additional redundancies in the A_1' and A_2" vibrations (sums of the in-plane and torsional angles, respectively) and in the E" mode are not shown. The G-matrix elements derived from these coordinates, with the assumption of 120^0 bond angles, are listed in Table 4.

The results of our normal coordinate analysis and force constant refinement are shown in Table 5. Agreement between observed and calculated frequencies is good, but again, the assumption of 120^0 bond angles will influence the calculated values to some extent. The stretch-stretch interaction constant is large, as might be expected for a ring structure. The frequency of the inactive A_2' mode is computed to be 570 cm^{-1}. Isotopic substitution of a single Si atom lowers the trimer symmetry to C_{2v} and induces activity of the A_2' mode. As diffusion proceeds and the trimer becomes more concentrated, structure develops in the 500-600 cm^{-1} region of the IR spectrum, part of which may be due to the activated A_2' mode.

The assignment of features at 621 cm^{-1} and 343 cm^{-1} to the torsional modes requires justification, particularly in the light of the assignment of the 79 cm^{-1} band to the torsional mode of the Si_2O_2 dimer by Hastie et. al. As stated earlier, Hastie et. al. observed no other absorption below 311 cm^{-1} which could be assigned to a torsional mode, which implies that the trimer torsional modes may have higher frequencies. This implication is further strengthened by the fact that the trimer, with 30 valence electrons, is isoelectronic with the benzene molecule. The ability of Si to form d_π-p_π bonds with second row non-metals results in multiple bonds of high strength. The cyclic structure thus provides a siloxane counterpart to benzene with delocalization and resonance of the oxygen lone pairs. This is expected to result in considerable resistance to out-of-plane deformation (which would decrease the resonance interaction.) Consequently, the out-of-plane torsional frequencies are expected to be high. The assignment of 621 cm^{-1} and 343 cm^{-1} features to these modes is, therefore, not unreasonable. In other planar species known to exhibit resonance (e.g. CO_3^{2-}, NO_3^-) the out-of-plane bending frequencies are in

the 800-900 cm^{-1} range [19]. In sym-d$_3$ benzene, which has the same
symmetry as Si$_3$O$_3$, the corresponding torsional modes have peaks at 693 cm^{-1}
and 373 cm^{-1} [20]. Delocalization and resonance usually result in enhanced
stability, so our observation of the persistence of the trimer features
after extended diffusion at 30K supports our interpretation.

D. Higher Order Multimers

As diffusion and reaction at 30K were continued up to eight hours, IR
features due to monomeric and dimeric SiO steadily decreased in intensity.
Trimeric features maintained growth, rapidly at first, then more slowly,
and then began to decrease at long diffusion times. These changes were
accompanied by the growth of weaker, broader peaks and a structured
continuous background absorption. Of the weak features, two which were
most sharp appeared at 1217.8 cm^{-1} and 763.0 cm^{-1}. While no definite
assignment can be made, it is assumed that these and most other features
are due to higher multimeric species. A number of peaks which were
assigned to a pentameric napthalene-like species were observed by Hastie
et. al. upon diffusion in the matrix or under non-ideal deposition
conditions. An alternate mechanism for the growth of high polymers and
transition to bulk material will be presented below.

E. Transition to Bulk SiO Residue

In the previous sections, it was noted that significant changes took
place in the absorption spectrum when the matrix was warmed to 30K and
diffusion permitted for several hours. In this section, the results of
further warmup to higher temperatures and sublimation of the nitrogen
support will be described. In the first part of these experiments,
diffusion at about 30K was permitted for eight hours. Infrared spectra
were recorded initially, then at intervals of two hours during the
diffusion period. (During this recording, the temperature of the matrix was
reduced to 12-15K to halt diffusion.) Following this, the matrix was
warmed to 32-33K (the temperature at which sublimation of the N$_2$ becomes

-12-

apparent) for two more two-hour periods. Finally, the matrix was warmed to about 50K until the nitrogen was completely sublimed and pumped away. The sample was recooled for recording of another spectrum, then was warmed slowly to room temperature under vacuum.

The initial deposit shows a flat background continuum with the prominent sharp monomer, dimer, and trimer absorptions superposed. A comparison of the expanded scale spectra with this figure indicates that there is essentially broad absorption in the region of 1000 cm^{-1}. Overlapping of at least four relatively narrow features cause a depressed continuum. As the sample diffuses at 30K, the low frequency limit of this depression gradually shifts from about 940 cm^{-1} to lower frequencies. After eight hours at 30K, the limit is about 905 cm^{-1}. The depth of absorption has increased slightly, but the appearance of new features at 984 cm^{-1} and 994 cm^{-1} prevent a precise determination of the shape of any broad underlying absorption. After two hours of diffusion at 32-33K, there is now a prominent absorption peaking at about 1000 cm^{-1} and spanning the 900-1300 cm^{-1} region. Weaker broad features occur between 800-900 cm^{-1} and between 300-500 cm^{-1}. The monomer line at 1224 cm^{-1} and the trimer feature at 972 cm^{-1} still appear. After four hours at 32K, the monomer line has disappeared and the trimer peak is weakly present. The spectrum is now quite similar to that found for smokes condensed from SiO vapor [4]. The main absorption maximum has shifted from 1000 cm^{-1} to 1050 cm^{-1}. The smoke spectrum is identical to that attributed to Si_2O_3 films [5].

After sublimation of the matrix at 50K and recooling to 12K, only broad features are seen in the infrared spectrum. The prominent absorption maximum now occurs at 960 cm^{-1} and the width has narrowed. After warming the matrix to room temperature, the CsI window was annealed at 6 hours at 200 $^{\circ}$C, resulting in further sharpening of this feature and an increase of the 450 cm^{-1} absorption. The residue is now essentially identical to that of the smoke condensate throughout the spectrum.

F. Mechanism of Residue Formation

SiO vapor condensation in inert, oxydizing, or reducing atmospheres [7] yielded fine smoke particles with neither bulk SiO_2 or SiC structure. Instead, the infrared spectrum was identical with that obtained from thin films of silicon deposited at low oxygen partial pressures. Microchemical analysis [5] gave the composition Si_2O_3.

Deposition of SiO in vacuum, i.e. oxygen pressure less than 10^{-5} torr, produces SiO films. However, small SiO grains formed by sublimation of an inert matrix at low temperatures are the same as the grains formed in the vapor. For the composition Si_2O_3 disproportionation of the SiO molecule must occur. In any case, a new silicon monoxide phase is produced.

This can be understood from the structural information obtained through the spectroscopic data reported here. As described above, the broad bands characteristic of Si_2O_3 grow at the expense of the monomer, dimer, and trimer peaks, an effect which must therefore happen due to diffusion controlled reaction between the smaller species. A reaction between Si_3O_3 and SiO results in the formation of an additional Si-O bond out of the trimer plane between a trimer Si and the monomer oxygen, with essentially free rotation about the new bond. Addition of a second SiO unit at the neighboring trimeric Si site yields an unstable structure due to the close encounter of the two new Si atoms. The result can be the loss of one of these Si atoms, and the formation of a bond between the remaining Si and O. A third monomeric unit can add to the final trimeric Si, losing another Si atom and forming a stable cage-like structure of composition Si_4O_6. This mechanism is schematically illustrated in Figure 5. The silicon atoms may become trapped inside the cage, resulting in some disorder. This structure can continue to grow by addition at the Si sites and produce a bulk material with net composition 1:1 Si:O, but with a skeleton having a ratio Si:O of 2:3. Our preliminary work on the electronic absorption spectrum indicates only broad and shallow absorption in the 200-300 nm region with no absorption due to free silicon. However, this may be due to a disordered cage structure.

-14-

Acknowledgements

References

[1] Proc. Int. Symp. on Condensation and Evaporation of Solids, ed. E. Rutner, P. Goldfinger, and J. Hirth (Gordon and Breach, New York) 1964

[2] R. C. Paule, High Temperature Science 8, 257 (1976)

[3] J. Turkevich, in Fundamental Phenomena in Material Sciences, Vol. 3, ed. L. J. Bonis, P. L. deBrune, and J. J. Duga (Plenum Press, New York) 1966

[4] K. L. Day and B. Donn, Science 202, 307 (1978)

[5] E. Ritter, Vak. Tech. 21, 42 (1972)

[6] Y. Nishimura and K. Inagaki, Fujitsu Sci. Tech. J. 2, 87 (1966)

[7] K. L. Day and B. Donn, Ap. Journal 222, L45 (1978)

[8] M. Moskovits and G. A. Ozin, Cryochemistry (Wiley and Sons, New York) 1976

[9] H. E. Hallam, ed., Vibrational Spectroscopy of Trapped Species (Wiley and Sons, New York) 1973

[10] A. J. Downs and S. C. Peake, in Molecular Spectroscopy, Vol 1 (The Chemical Society, London) 1973

[11] W. Schulze, H. U. Becker, and D. Leutloff, J. de Physique Coll. 38, C2-7 (1977)

[12] M. Moskovits and J. E. Hulse, J. Chem. Phys. 67, 4271 (1977)

[13] J. S. Anderson, J. S. Ogden, and M. J. Ricks, Chem. Comm. 1968, 1585 (1968)

[14] J. S. Anderson and J. S. Ogden, J. Chem. Phys. 51, 4189 (1969)

[15] J. W. Hastie, R. H. Hauge, and J. L. Margrave, Inorg. Chim. Acta 3, 601 (1969)

[16] A. B. Anderson, Private communications

[17] G. Herzberg, Molecular Spectra and Molecular Structure I. Diatomic Molecules (Prentice-Hall, New York) 1939

[18] M. G. Voronkov, V. P. Mileshkevich, and Yu. A. Yuzhelevskii, The Siloxane Bond (Consultants Bureau, New York) 1978

[19] K. Nakamoto, Infrared Spectra of Inorganic and Coordination Compounds, 2nd. ed. (Wiley-Interscience, New York) 1970

[20] F. A. Miller and B. L. Crawford, J. Chem. Phys. 14, 282 (1946)

Table 1. Results of force constant refinement calculations

Structure and parameters
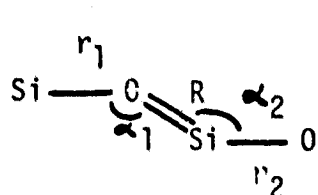
$$r_1 = r_2 = 1.74 \text{ Å}$$
$$R = 1.51 \text{ Å}$$
$$\alpha_1 = \alpha_2 = 109^{\circ} \ 28'$$

Calculated force constant matrix ($\underline{F}$-matrix)

(a)

$$\underline{F} = \begin{bmatrix}
 & r_1 & R & r_2 & \alpha_1 & \alpha_2 & \\
 & 3.85 & 1.57 & (0.0) & 0.017 & (0.0) & r_1 \\
 & & 9.27 & 1.57 & 0.024 & 0.024 & R \\
 & & & 3.85 & (0.0) & 0.017 & r_2 \\
 & & & & 0.452 & (0.0) & \alpha_1 \\
 & & & & & 0.324 & \alpha_2
\end{bmatrix}$$

Observed and calculated $^{28}Si_2^{16}O_2$ frequencies (cm^{-1})

$\nu_{obs.}$	$\nu_{calc.}$	Assignment
1221.5	1221.5	Si=O stretch
804.4	804.4	Si-O stretch
765.5	765.5	Si-O stretch
252.	252.0	bend
--	180.3	bend
79.(b)	--	torsion

Notes:

(a) All force constants are expressed in units of mdyne/Å.
(b) Data of Hastie et. al. [3]
(c) All in-plane modes are of symmetry species A' and the torsional mode is of species A", assuming C_s symmetry.

Table 2: Observed and calculated frequencies for Si_2O_2 isotopic variants

Isotopic species	$\nu_{obs.}$	$\nu_{calc.}$
$^{28}Si-^{16}O$ \ $^{28}Si-^{16}O$	1221.5	1221.5
	804.4	804.4
	765.5	765.5
	252.	252.0
	--	180.3
	79. (a)	--
$^{28}Si-^{16}O$ \ $^{28}Si-^{18}O$	--	1219.7
	791.3 (b)	799.1
	749.4	744.7
	--	248.1
	--	177.0
$^{28}Si-^{18}O$ \ $^{28}Si-^{16}O$	--	1178.6
	791.3 (b)	788.5
	749.4	751.0
	--	250.7
	--	179.5
$^{28}Si-^{18}O$ \ $^{28}Si-^{18}O$	--	1176.6
	776.2 (b)	774.6
	739.0	738.8
	--	246.1
	--	175.1
$^{28}Si-^{16}O$ \ $^{29}Si-^{16}O$	--	1214.3
	802. (sh)	803.2
	760.5	761.3
	--	251.1
	--	179.3
$^{29}Si-^{16}O$ \ $^{28}Si-^{16}O$	--	1221.3
	799.0	801.0
	763.0	764.4
	--	250.2
	--	179.7
$^{28}Si-^{16}O$ \ $^{30}Si-^{16}O$	--	1207.5
	802. (sh)	802.3
	760.5	757.1
	--	250.2
	--	178.4

	(a)	(b)
$^{30}Si{-}^{16}O$	--	1221.2
	799.0	798.0
$^{28}Si{-}^{16}O$	763.0	763.3
	--	248.6
	--	179.1

Notes:
(a) Data of Hastie et. al. [3] for Si_2O_2 in Ar.

(b) Data of Anderson and Odgen [2] for Si_2O_2 in N_2.

All frequencies expressed in cm^{-1}. Absolute frequency accuracy is estimated at 0.2 cm^{-1} for data of the current study.

Table 3: F-matrix for Si_3O_3 with D_{3h} symmetry

$$F(A_1') = \begin{bmatrix} F_R+2F_{RR}+2F_{RR'} & 0 \\ & F_\alpha \end{bmatrix}$$

$$F(A_2') = F_R-2F_{RR}+F_{RR'}$$

$$F(A_2'') = F_\delta-2F_{\delta\delta}$$

$$F(E') = \begin{bmatrix} F_\alpha-F_{\alpha\alpha} & -F_{\alpha\alpha} & \sqrt{2}F_{R\alpha} & (-\sqrt{2}/2)F_{R\alpha} \\ & F_\alpha-F_{\alpha\alpha} & (-2/\sqrt{2})F_{R\alpha} & \sqrt{2}F_{R\alpha} \\ & & F_R+(1/2)F_{RR}-F_{RR'} & (-1/2)F_R-F_{RR}+(1/2)F_{RR'} \\ & & & F_R+(1/2)F_{RR}-F_{RR'} \end{bmatrix}$$

$$F(E'') = F_\delta-F_{\delta\delta}$$

Note: The usual conventions for denoting major and interaction constants apply. Species designations are shown at the left of the table.

Table 4: G-Matrix Elements for Si_3O_3 Trimer of D_{3h} Symmetry

$$G(A_1') = \begin{bmatrix} (1/2)(\mu_{Si} + \mu_0) & (-\sqrt{3})(\mu_{Si} - \mu_0) \\ & 6(\mu_{Si} + \mu_0) \end{bmatrix}$$

$$G(A_2') = (3/2)(\mu_{Si} + \mu_0)$$

$$G(E') = \begin{bmatrix} 3(\mu_{Si} + \mu_0) & (3/2)(\mu_{Si} + \mu_0) & (-3/\sqrt{6})(\mu_{Si} + \mu_0/2) & (3/2\sqrt{6})(\mu_{Si} - \mu_0) \\ & 3(\mu_{Si}/2 + \mu_0) & (-3/2\sqrt{6})(\mu_{Si} - \mu_0) & (-3/\sqrt{6})(\mu_{Si}/2 + \mu_0) \\ & & (1/2)(\mu_{Si} + 5\mu_0/2) & (-1/4)(\mu_{Si} + \mu_0) \\ & & & (1/2)(5\mu_{Si}/2 + \mu_0) \end{bmatrix}$$

$$G(A_2'') = 24(\mu_{Si} + \mu_0)$$

$$G(E'') = 8(\mu_{Si} + \mu_0)$$

Note: Symmetry designations are shown to the left of the Table.

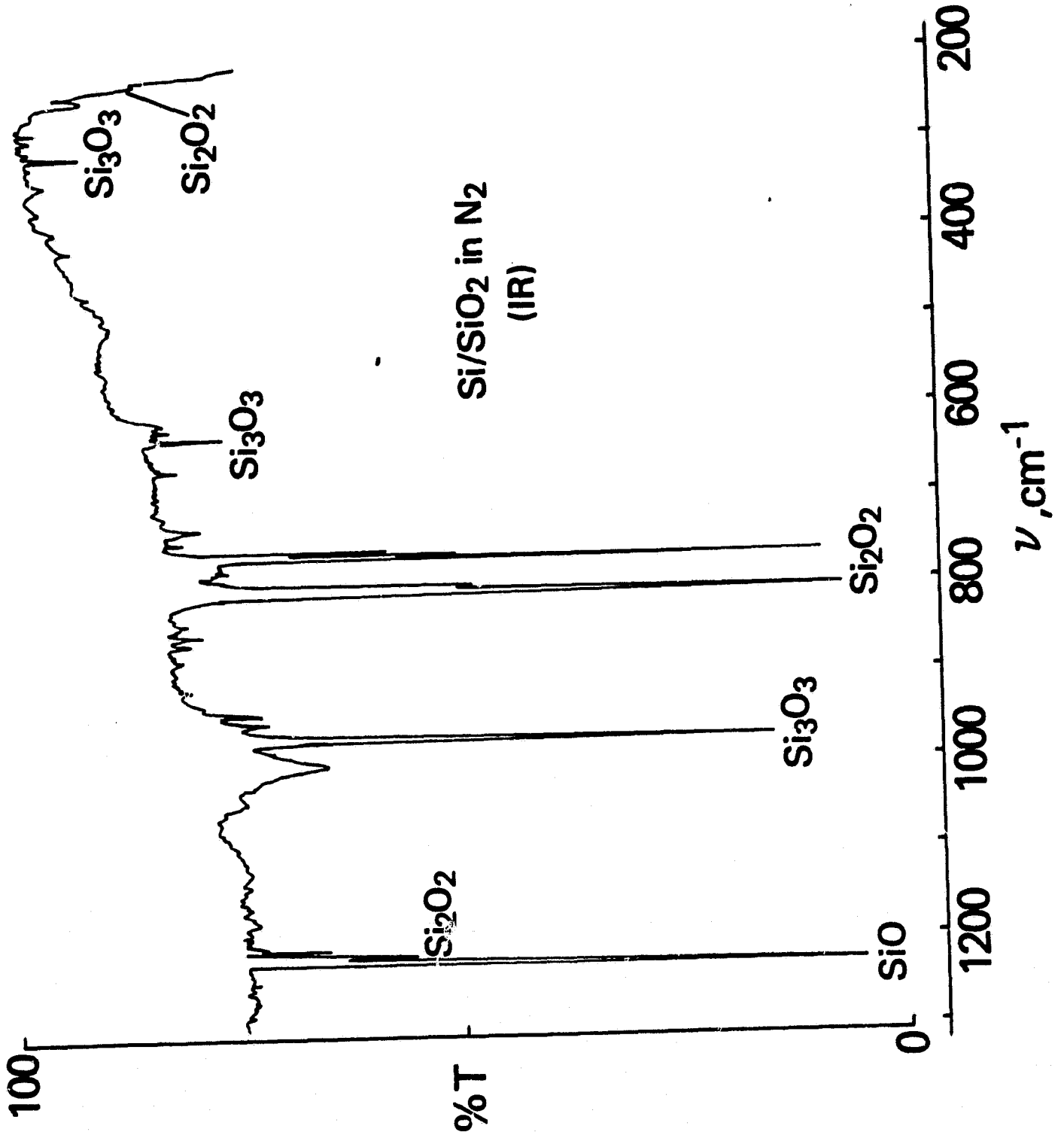## Table 5: Results of Normal Coordinate Analysis for Si_3O_3 (D_{3h})

A. Observed and Calculated Frequencies (cm^{-1})

Species	$^{28}Si_3\,^{16}O_3$ Observed	$^{28}Si_3\,^{16}O_3$ Calculated
A_1'	675	675.0
	458	458.0
A_2'	---	570.9
E'	972.2	972.6
	630.5	630.8
	311.0	311.0
A_2''	621.0	(621.0)
E''	343	(343.0)

B. Force constants ($md/\text{Å}$)

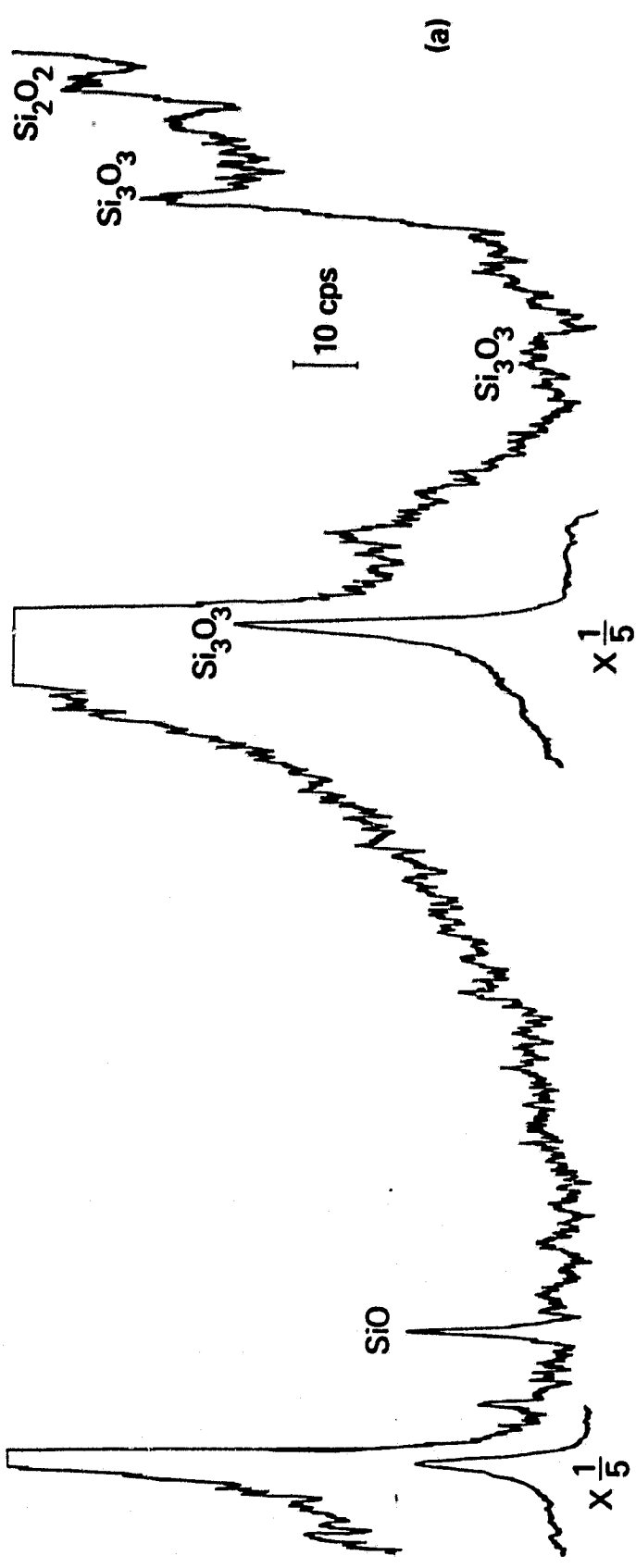|					
F_R	6.98	F_α	0.25	F_δ	0.87
F_{RR}	-1.98	$F_{\alpha\alpha}$	-0.025	$F_{\delta\delta}$	-0.045
$F_{RR'}$	1.04	$F_{R\alpha}$	0.34		

Figure 1:   Infrared spectrum of the Co-deposition of vapors of an equimolar Si, SiO_2 mixture with a stream of N_2 gas on a substrate at 12K.

Figure 2:   Infrared spectra of SiO species in N_2 matrix recorded after successive periods of diffusion at 30K. (a) After 2 hours, (b) After 4 cumulative hours, (c) After 6 cumulative hours. The matrix was cooled to 12K after each diffusion period for each tracing.

Figure 3:   (a) Raman Spectra of SiO species in a N_2 matrix at 12K using 488.8 nm excitation. (b) Raman spectrum after 1.5 hours of diffusion at 30K.

Figure 4:   Transition from molecular to bulk material monitored using infrared spectroscopy. (a) After 8 hours at 30K plus an additional 2 hours at 32K. (b) After 8 hours at 30K plus 4 hours at 32K. (c) After warming the sample to $\sim$ 50K and subliming the N_2 host matrix. (d) After 3 days at room temperature in the evacuated cell. (e) After annealing the residue at 500K for 6 hours

Figure 5:   Mechanism for growth of bulk material of composition Si_2O_3. Units of SiO are attached successively to the starting Si_3O_3. With each addition a new SiO bond is formed and a Si atom is lost. The cage structure Si_4O_6 continues to grow by formation of additional SiO linages.
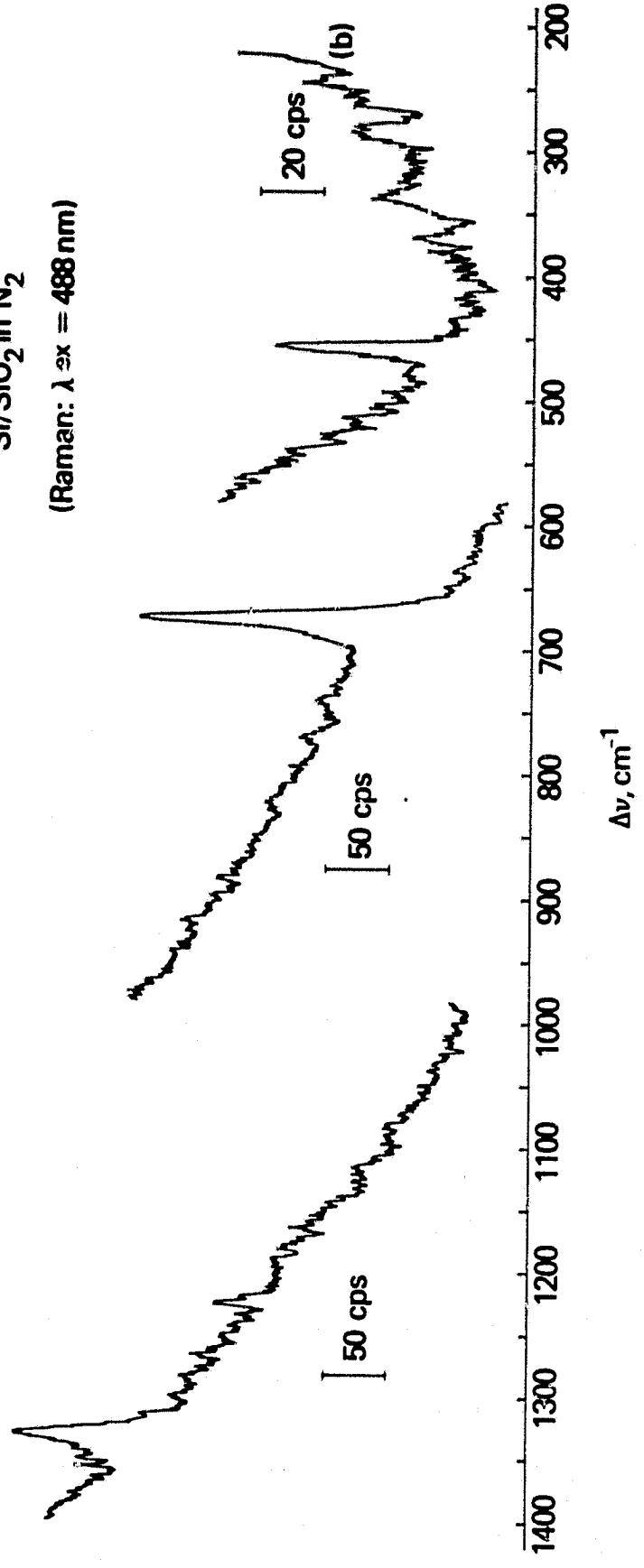
Si/SiO$_2$ in N$_2$ (IR)

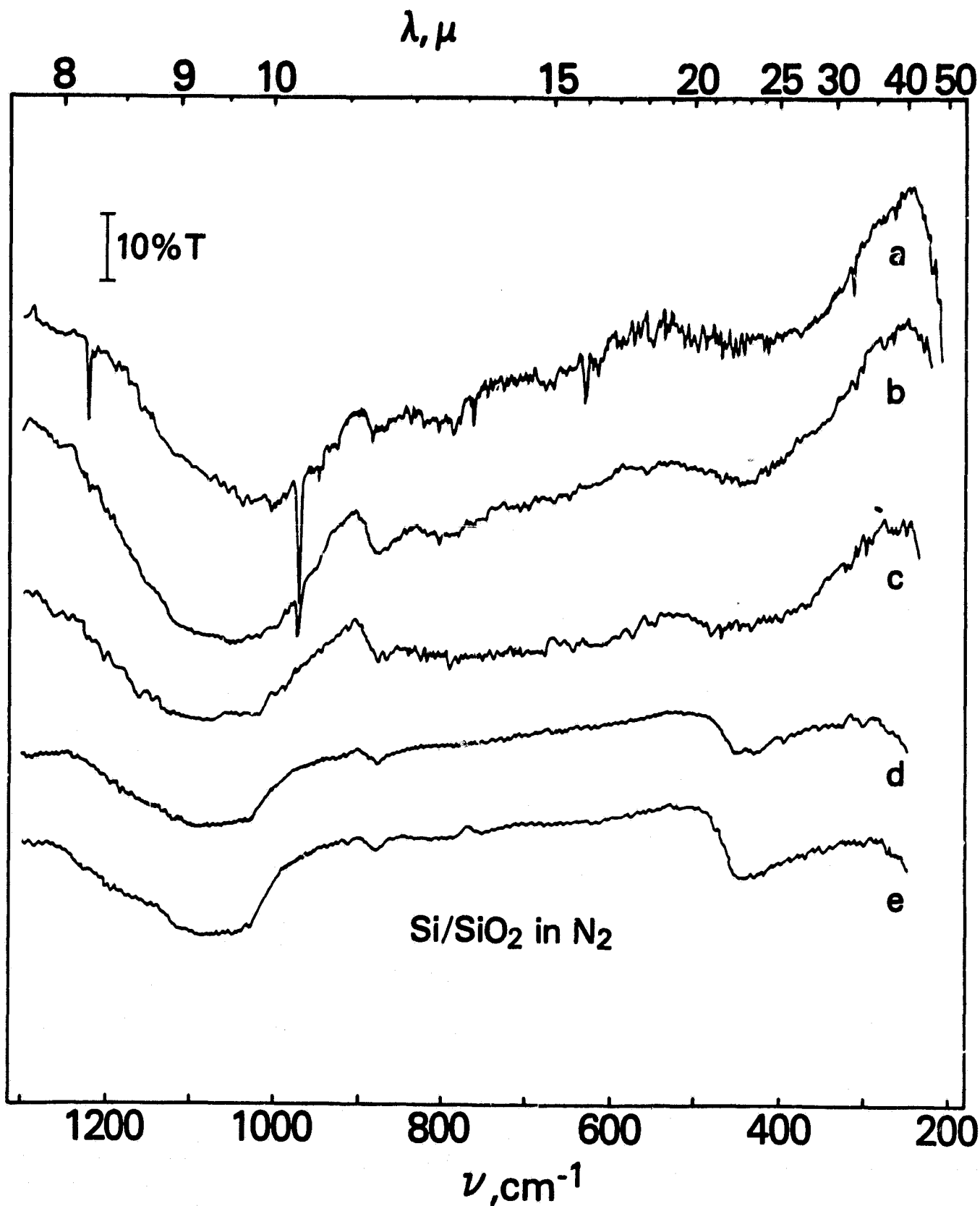%T

ν ,cm^{-1}

Si$_3$O$_3$
Si$_2$O$_2$
Si$_3$O$_3$
Si$_2$O$_2$
Si$_3$O$_3$
Si$_2$O$_2$
SiO

Si/SiO$_2$ in N$_2$ (IIR)

ν, cm^{-1}

Si$_3$O$_3$

Si$_2$O$_2$

Si$_3$O$_3$

SiO

Si$_2$O$_2$

10%T

Si/SiO$_2$ in N$_2$

(Raman: $\lambda_{ex} = 488$ nm)

(a)

(b)

Si_2O_2

Si_3O_3

Si_3O_3

Si_3O_3

SiO

10 cps

20 cps

50 cps

50 cps

50 cps

$\times \frac{1}{5}$

$\times \frac{1}{5}$

$\times \frac{1}{5}$

$\Delta \nu$, cm^{-1}

200   300   400   500   600   700   800   900   1000   1100   1200   1300   1400

λ, μ

8 9 10 15 20 25 30 40 50

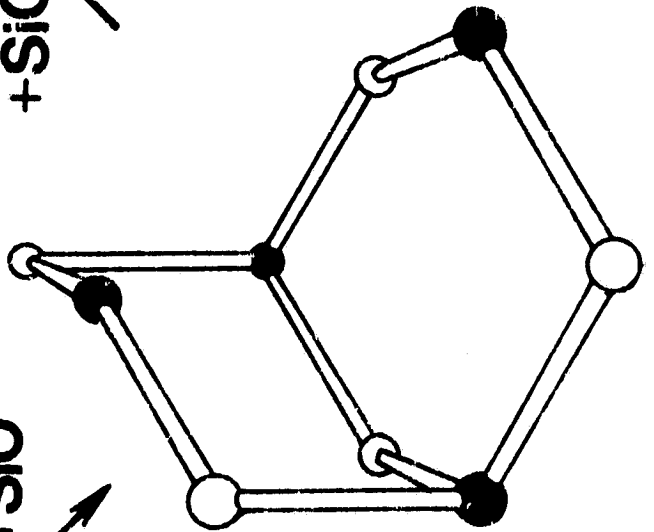$\boxed{\text{10\%T}}$

a

b

c

d

e

Si/SiO$_2$ in N$_2$

1200 1000 800 600 400 200

ν, cm^{-1}
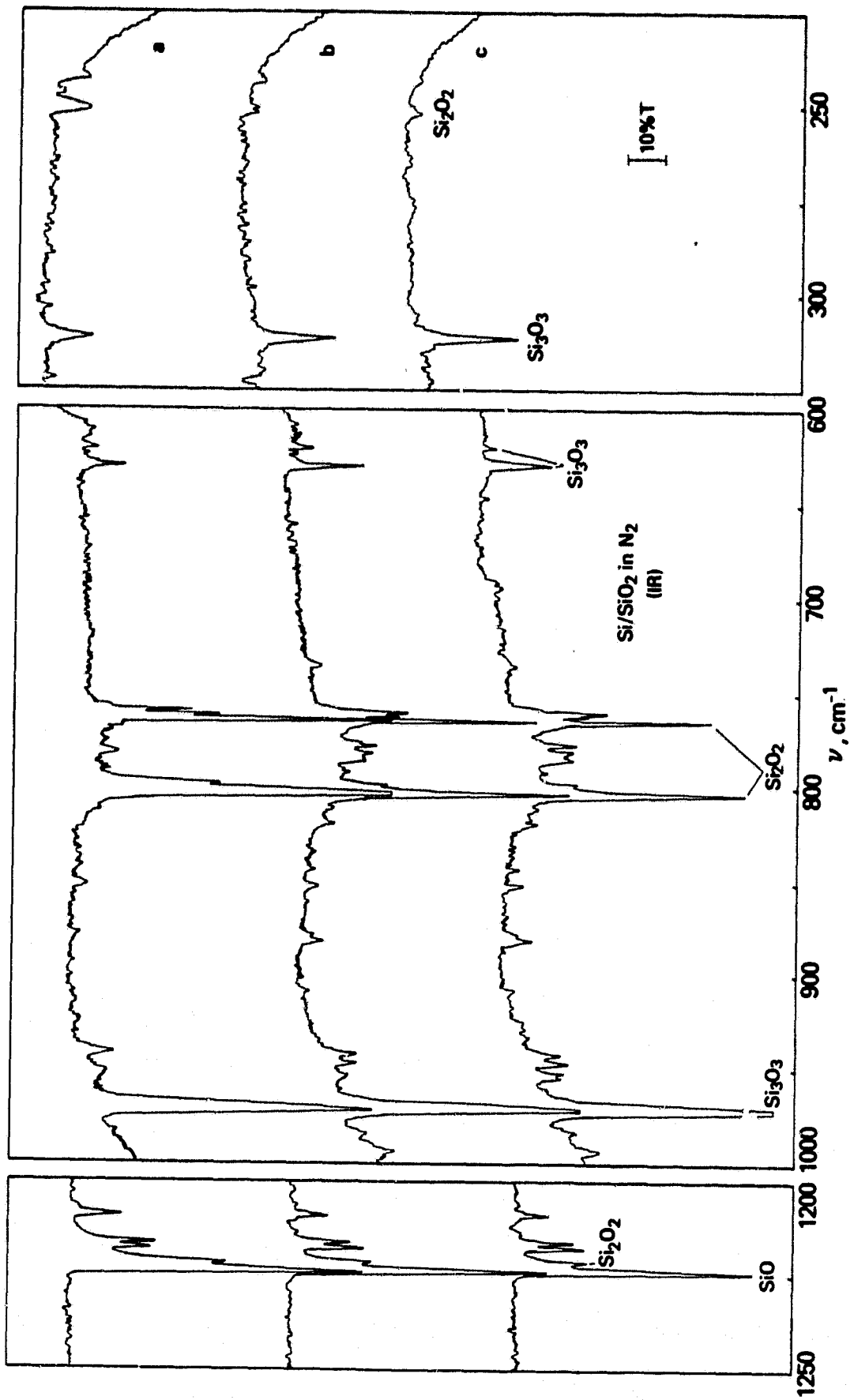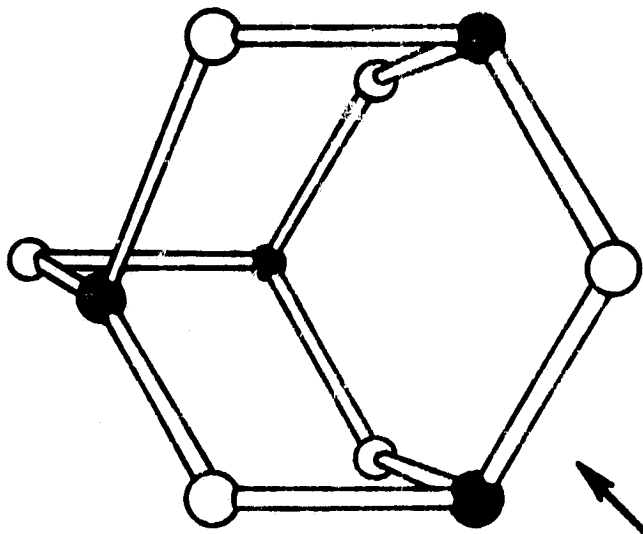
Oxygen
Silicon

+SiO
−Si

+SiO
−Si